CrystEngComm

ROYAL SOCIETY OF CHEMISTRY

COMMUNICATION

View Article Online
View Journal

Cite this: DOI: 10.1039/d6ce00284f

Received 9th April 2026,
Accepted 26th May 2026

DOI: 10.1039/d6ce00284f

rsc.li/crystengcomm

Oblique-angle deposition of self-assembled zigzag-shaped Au nanostructures in $La_{0.7}Sr_{0.3}MnO_3$–Au vertically aligned nanocomposite thin films

Benson Kunhung Tsai,[a] Jialong Huang,[a] Abhijeet Choudhury,[a] Allison Nobuko Scher,[a] Jeremy B. Gan,[a] Peter Bermel *[b] and Haiyan Wang *[ab]

Hyperbolic metamaterials (HMMs) provide a unique tailorable material platform to manipulate light–matter interactions, which traditional single-phase materials cannot achieve easily. Typical HMMs possess a periodic array of metallic nanopillars embedded within a dielectric matrix material. As a new class of HMMs, vertically aligned nanocomposites (VANs) demonstrate uniformly distributed, vertically aligned metallic nanopillars in an oxide matrix *via* a self-assembly deposition process. Herein, by combining oblique-angle deposition (OAD) and multilayer VAN growth, zigzag-shaped metallic nanopillars within an oxide matrix have been demonstrated. Specifically, by changing the oblique angle in each layer during multilayer Au–$La_{0.7}Sr_{0.3}MnO_3$ VAN growth, zigzag-shaped Au nanopillars are embedded within the $La_{0.7}Sr_{0.3}MnO_3$ matrix. Interestingly, by varying the inclination angles of the substrate and utilizing the shadowing effect during OAD, tailorable Au nanostructures and tunable anisotropic optical properties have been demonstrated. This new OAD–VAN combined deposition method presents great potential for the design and processing of very complex 3D HMMs for future integrated photonic devices.

Introduction

Optical metamaterials with epsilon-near-zero (ENZ) permittivity characteristics show tremendous potential for photonic devices.[1,2] One approach to obtain ENZ and hyperbolic dispersion is to create hyperbolic metamaterials (HMMs) with an array of metallic nanopillars embedded in a dielectric matrix,[3] which leads to optical anisotropy, where one principal direction exhibits metallic behavior and the other dielectric behavior. These special nanostructured thin-film materials can be found in various types of applications, such as sensing,[4] spontaneous emission,[5] and superlenses.[6] The most well-demonstrated HMMs include electro-deposition of Au or Ag within anodic aluminum oxide[7,8] and lithography-patterned metallic nanostructures in oxides. Typically, the size of the nanowires is limited by the size of the anodic aluminum oxide template or the lithographic patterning resolution, in the range of 100 nm to a few microns depending on the methods applied.

Vertically aligned nanocomposites (VANs) refer to a new class of nanocomposite thin films that combine two materials in a nanopillar-in-matrix form. VANs have recently gained significant attention due to their anisotropic properties,[9] vertical interface coupling,[10] and multifunctionality.[11–13] One classical VAN example is achieving multiferroicity by incorporating a magnetic material, such as $CoFe_2O_4$ (ref. 14) or Fe,[15] into a ferroelectric $BaTiO_3$ (BTO) matrix. Furthermore, incorporating metals as nanopillars within the matrix can result in magnetic and optical anisotropy.[3,10] The strong vertical interface coupling between magnetic metals and plasmonic materials can result in magneto-optical coupling. Additionally, these fascinating optical metamaterials can be tailored into 3D nanostructures, involving VANs with a multilayer design.[16,17] The selection of multiple materials, along with the addition of 3D nanostructures to tailor thin-film properties, shows enormous potential for device applications.

Oblique-angle deposition (OAD) is a deposition technique in which the substrate is tilted towards the plume impinging direction. Because of this tilted growth, OAD typically results in tilted columnar thin films due to the shadowing effect and limited adatom diffusion.[18] By varying the rotation speed and controlling the substrate holder, the resulting nanostructures can be in zigzag, S-shaped, or helical forms.[19] With the development of OAD, a wide range of single-phase materials have been synthesized and applied in various fields, such as in electrochemical, sensor, and optical devices.[20]

[a] School of Materials Engineering, Purdue University, West Lafayette, Indiana 47907, USA. E-mail: hwang00@purdue.edu
[b] School of Electrical and Computer Engineering, Purdue University, West Lafayette, Indiana 47907, USA

Traditionally, OAD has been applied only to single-phase materials, with very few successes in two-phase VAN systems. The nanostructure morphology of the thin film differs from that of traditional OAD, resulting in tilted Au nanopillars within a Li_2MnO_3 (LMO) matrix. Since Au is an effective current collector in VAN thin films, the LMO–Au system can function as an effective cathode for thin-film battery applications.[21]

In this work, a combined OAD and multilayer-VAN method was proposed to deposit complex 3D Au nanostructures in a $La_{0.7}Sr_{0.3}MnO_3$ (LSMO)-based VAN thin film. After the first layer of the LSMO–Au thin film was deposited, the substrate holder was rotated 180° for the next layer. Such alternating OAD deposition angle could result in a zigzag film morphology, as illustrated schematically in Fig. 1. The inclination angle for the substrate and the thicknesses of each layer could also be adjusted. The nanostructures of all thin films were analyzed using scanning transmission electron microscopy in high-angle annular dark-field mode (HAADF-STEM) coupled with energy-dispersive X-ray spectroscopy (EDS) for elemental mapping. Furthermore, the optical properties of the thin films were tested to explore the angular dependence of the optical response both in plane and out of plane.

Results and discussion

Here, a series of LSMO–Au thin films were first deposited on to $SrTiO_3$(001) (STO) substrates using different inclination angles of the substrate holder in an oblique-angle deposition (OAD) configuration. Previously, LSMO–Au VAN thin films with Au nanopillars have been reported on STO(001) substrates under normal-incidence deposition without substrate inclination.[22–24] Uniform Au nanopillars with tunable pillar density can be achieved by adjusting the Au composition in the LSMO–Au nanocomposites. Based on the strain compensation model for VAN growth,[25] the opposite in-plane strain state at the matrix-substrate and the pillar–substrate interfaces can promote improved in-plane ordering of the pillars. Since LSMO has a pseudocubic structure with a = 3.873 Å, Au has a cubic structure with a = 4.072 Å, and STO has a cubic structure with a = 3.905 Å, the LSMO–Au/STO system approximately satisfies the perfect strain compensation condition, *i.e.*, in-plane tensile strain at the LSMO/STO interface and in-plane compressive strain at the Au/STO interface.[22] To obtain a zigzag nanostructure from OAD, we propose to grow a three-layer VAN stack thin film with alternating inclination directions. The substrate holder was rotated by 180° between successive layers to reverse the incident flux direction and facilitate zigzag-shaped pillar formation. To examine the crystallinity and out-of-plane texture of the thin films, θ–2θ XRD measurements were first performed. The results are shown in Fig. S1. The XRD results reveal an obvious LSMO (200) peak, whereas the Au-related peaks are not distinctly resolved. The weak Au signal might be due to the shadowing effect during OAD, which could modify the crystallinity of the Au pillars and continuity compared to previous results.[26,27] Furthermore, the LSMO (200) peak systematically shifts to higher 2θ values as the inclination angle of the substrate increases from 15° to 45°, which suggests a reduced out-of-plane d-spacing for LSMO, as shown in Fig. S2. This trend is primarily attributed to a reduced vertical strain coupling at the LSMO–Au vertical interfaces under OAD, as tilted/discontinuous Au pillars can weaken strain transfer and diminish the strain-compensation effect. Other factors that can affect the LSMO lattice (*e.g.*, oxygen nonstoichiometry) were also considered. Because the oxygen partial pressure and growth temperature were kept constant across samples, an inclination-driven change in oxygen vacancy concentration is less likely to be the dominant cause of the systematic (200) shift. There was no obvious film peak observed for the 60° OAD deposition, where the nanostructure may have been altered by such a high inclination angle of the substrate, leading to a substantially weakened diffraction signal in the θ–2θ geometry.

Following the XRD analysis, a detailed microstructural analysis was conducted on these OAD samples using STEM-HAADF. Since the VAN thin film was deposited in an oblique-angle configuration, the shadowing effect should be considered as well, which could potentially alter the nanostructures over a large sample area.[20] Thus, two different regions of the thin film on the substrate were examined. Here, the bottom is defined as the substrate that is closer to the substrate holder and farther from the plume,

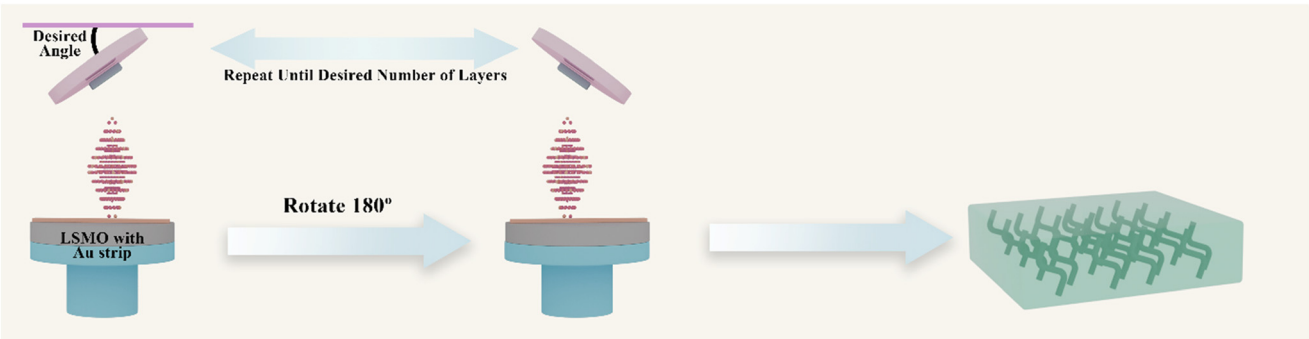

Fig. 1 Schematic of oblique-angle deposition used to synthesize zigzag $La_{0.7}Sr_{0.3}MnO_3$–Au vertically aligned nanocomposites.

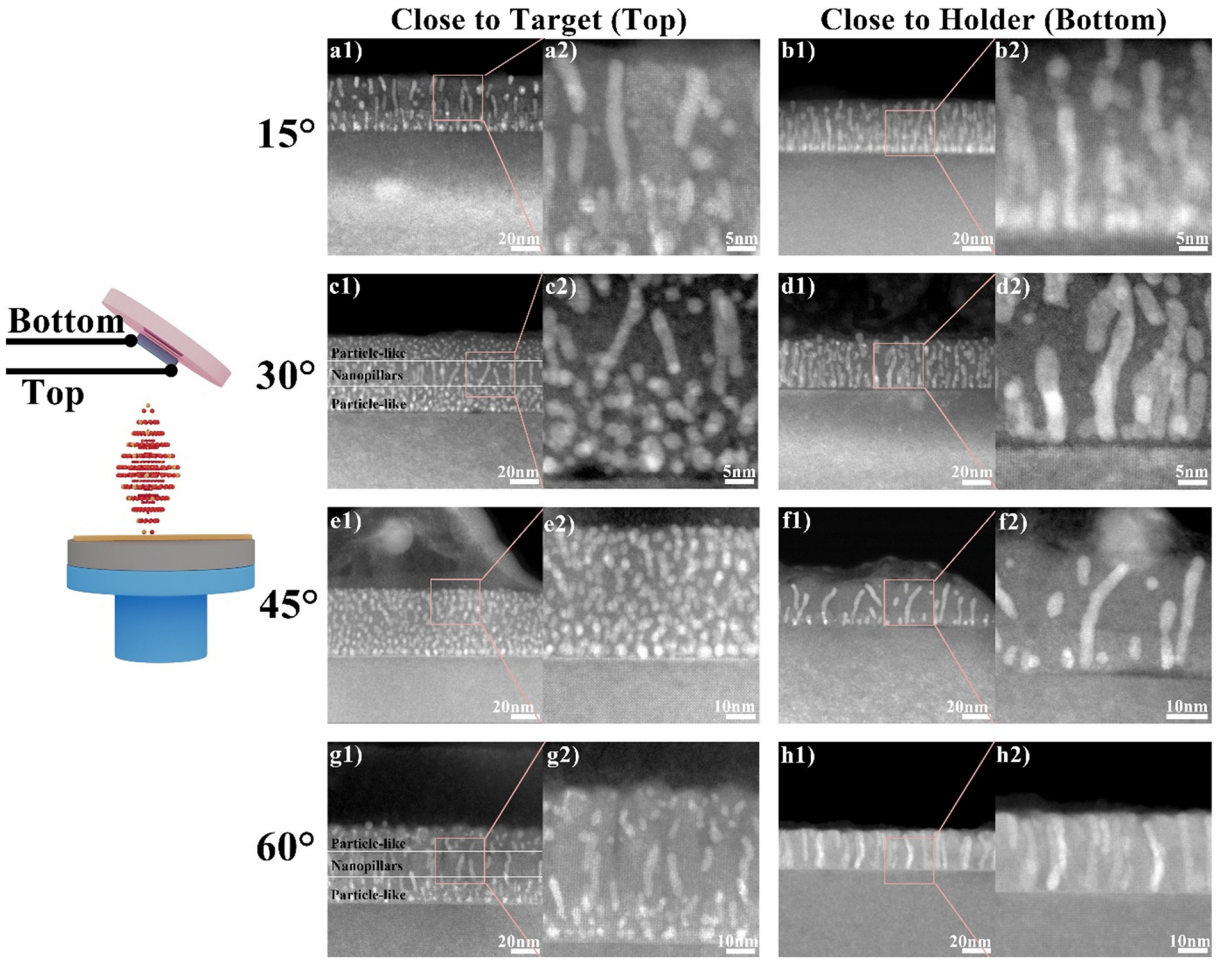

Fig. 2 High-angle annular dark field scanning transmission electron microscopy (HAADF-STEM) images of VAN thin film deposits under different inclination angles.

and the top is defined as the substrate closer to the target and the plume, as shown in Fig. 2. All corresponding STEM-EDS elemental mappings are shown in Fig. S3 and S4 to confirm the composition ratio of LSMO and Au within the thin films. All films show LSMO as the matrix and Au as nanopillars, which is similar to previous reports.[22,23] With the lowest angle of 15°, some of the nanopillars have resulted in zigzag shape in the bottom portion of the film as shown in Fig. 2(a1). Interestingly, the top portion of the film does not result in zigzag-shaped Au; instead, it shows a nanopillar shape as shown in Fig. 2(a2). By increasing the inclination angle of the substrate to 30° for the deposition, Au shows an interesting nanostructure evolution as the film grows. The initial deposition at the bottom of the substrate results in more nanoparticle formation for the first 18.7 nm of the film; in the next 14.1 nm, nanopillars are formed, followed by nanoparticle formation in the remaining portion of the film. Such thickness-dependent evolution is not seen in the bottom portion of the film as shown in Fig. 2(d1 and d2). The bottom portion of the thin film exhibits a more zigzag-like nanostructure mixed with some nanopillars as shown in Fig. 2(d2). On further increasing the substrate angle to 45° and 60°, similar to the case of the 30° angle, the bottom portion of the 45° and 60° thin films clearly shows a zigzag-like nanostructure of Au. The top portion of the thin films also behaves similarly to those that formed at the substrate angle of 30°, where no clear zigzag-like Au nanostructure is seen.

A previous VAN study has shown that the thickness effect of VAN samples affects the aspect ratio of the metal nanostructures and thus the overall optical properties of thin films.[10] Furthermore, as the thickness increases in OAD growth, the shadowing effect on the substrate increases, which might potentially affect the VAN nanostructure as the thickness increases. Thus, thickness-dependent deposition has also been implemented at different parts of the thin film, as shown in Fig. 3. The inclination angle of the substrate was selected as 30° as the zigzag shape could be synthesized at this angle, as shown in Fig. 3(a). Three layers of thin film was applied. Overall, all three thickness samples showed well-grown thin films without any columnar growth that was typically reported in single-phase OAD growth throughout the entire film thickness. The resulting thickness for a medium film is around 80 nm. Different

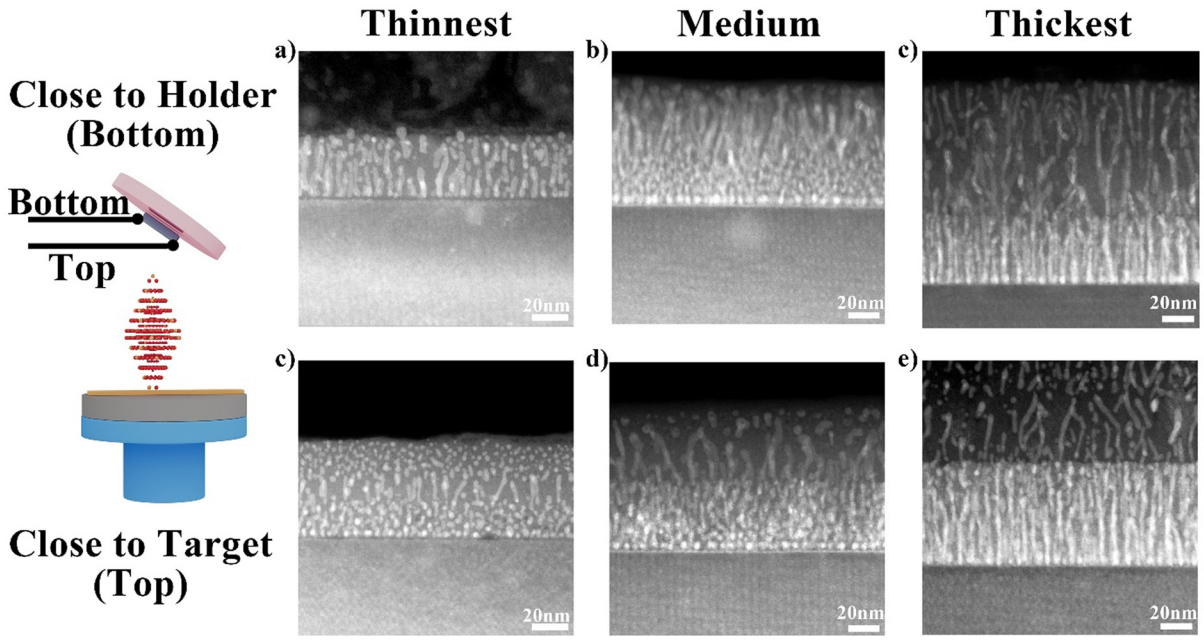

Fig. 3 Thickness dependence for 30° of inclination angle deposition. a–e) HAADF-STEM images of the top and bottom portions of the thin film.

from that of the thinnest one, the bottom portion of the medium-thickness film does not show a clear nanostructure revolution. Au is deposited in a zigzag shape within the thin film, but the structure does not continuously grow from the bottom to the top. For the top portion of the medium-thickness thin film, more tilted nanopillars are formed than zigzag Au nanopillars in the remaining portion of the film. Next, the thickest film is around 130 nm in thickness. The bottom portion of the thick film shows straight Au nanopillars with minor tilting in the initial growth. As the thickness increases, the nanopillars start to show a zigzag shape. The Au nanostructures are discontinuous throughout the film thickness. The top portion of the thick film shows a more nanopillar-like structure with a minor tilting angle throughout the film thickness.

Optical properties of various inclination angle-dependent thin films were also explored. The optical transmittance spectrum is shown in Fig. S4. Most previously reported VAN films show an interesting transmittance peak near the visible wavelength of light.[16,17,28] All VAN films prepared *via* OAD exhibit two transmittance peaks located at around 486 nm and 552 nm for all samples. These two different peaks could be attributed to the different sizes of the zigzag-shaped Au nanostructures that have been exposed to light, as shown in Fig. 2. To further investigate the optical properties of all films, spectroscopic angular-dependent ellipsometry measurements were performed, and ψ and Δ were collected. To obtain the optical permittivity, the data were fitted using a B-spline model. The wavelength measured ranges from 300 nm to 2500 nm. The anisotropic properties were observed in all films, as shown in Fig. 4(a), where the real permittivity behaves differently between in plane ($\varepsilon_{\parallel}$) and out of plane ($\varepsilon_{\perp}$). In addition, all films exhibit type-I hyperbolic behavior[10] where $\varepsilon_{\parallel} > 0$ and $\varepsilon_{\perp} < 0$. All films show dielectric-like behavior when $\varepsilon_{\parallel} > 0$. Thin films deposited at different inclination angles exhibit epsilon-near-zero (ENZ) behavior at different wavelength regimes. Specifically, the 15° deposited thin film shows ENZ wavelengths at 358 nm and 935 nm, while the 60° deposited thin film shows ENZ wavelengths at 392 and 473 nm. Furthermore, the 30° and 45° deposited thin films show ENZ wavelengths at 1126 and 1102 nm, respectively.

Additionally, optical reflectivity was tested for all films deposited at different inclination angles. Fig. 4(b–d) show the reflectance spectra of the substrate-angle-dependent thin films with different incident angles of light (30–70°). The overall reflectance increases as the incident angle of light increases from 30° to 70°. The spectra for 15° and 30° do not show any significant peaks throughout the spectrum. When the substrate angle for deposition increased to 45°, a significant peak appeared at 520 nm. Additionally, when the angle increased to 60°, the peak disappeared again. This significant peak could potentially represent localized plasmonic resonance. Previously, tilted nanopillar type VANs have shown different responses in reflectance spectra with positive and negative angles of incident light.[28] Here, the 45° thin film was rotated in-plane to obtain positive and negative angles of incident light. The positive incident light occurs when the substrate is tested under 0° and 90°, as illustrated in the inset. The negative incident light occurs when the substrate is rotated to 180° and 270°.

The optical permittivity results show the impact of the ENZ wavelength on Au pillar morphology and filling fraction, especially in the out-of-plane response. At 30–45°, the more continuous zigzag Au pillars likely allow for a stronger out-of-plane metallic character, leading to an ENZ wavelength in the near-infrared (~1100 nm) region, while at 15° and 60°, the

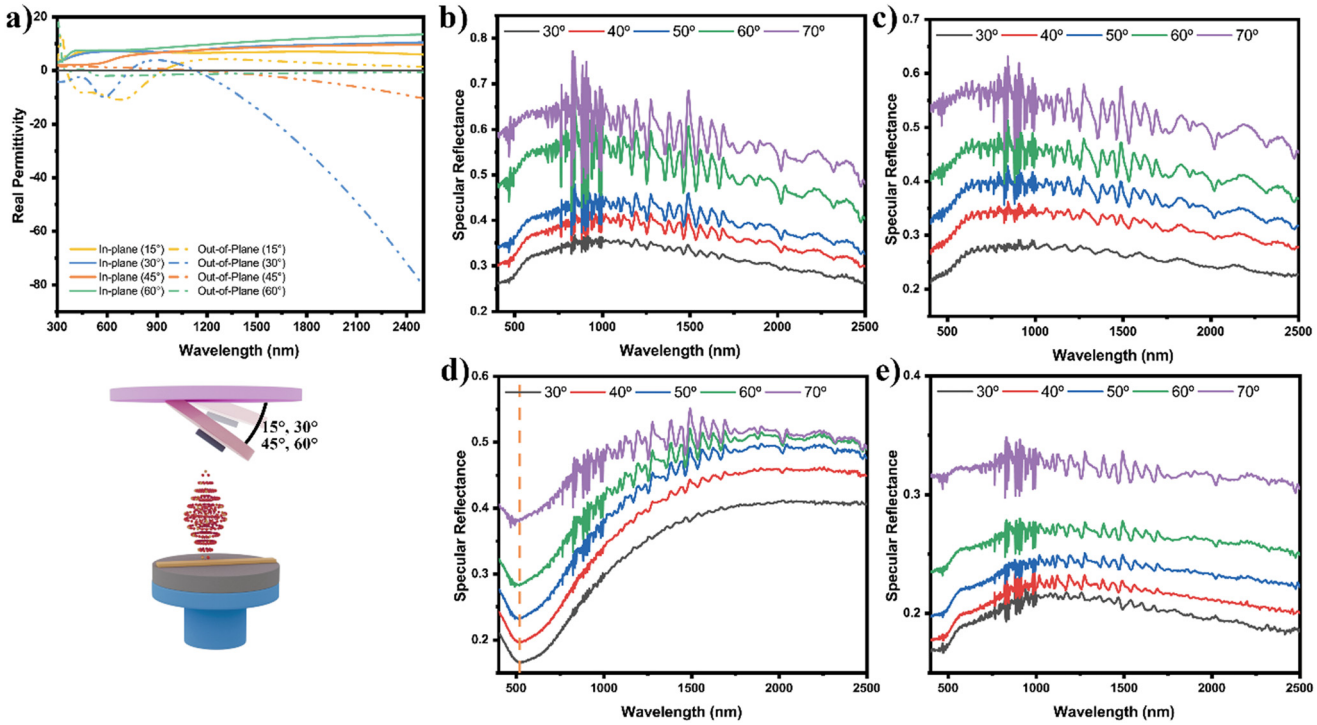

Fig. 4 Spectroscopic ellipsometry and reflectivity measurements of thin film deposition at different inclination angles. a) Optical permittivity for the real part and b–e) reflectivity measurements.

shadowing effect likely reduced pillar continuity, bringing $\varepsilon_{\perp}$ closer to $\varepsilon_{\parallel}$. As depicted in Fig. 4(b–e), the reflectance increases with increasing incident angle for all samples, and the reflectance peak at ~520 nm observed only for the 45° sample is consistent with a plasmonic response supported by relatively well-formed Au nanostructures. With the unique tilted nanostructures in the thin film, the sample could potentially respond differently when rotated in-plane. The reflectance spectra measured, as shown in Fig. 5 with the insets showing the measured sample position and angle relative to the incident beam, also showed a similar trend, with the reflectance peak staying at ~520 nm without any regard for the in-plane rotation angle. This result suggests that the optical response of the zigzag Au nanostructures does not exhibit a strong dependence on the in-plane orientation of the sample.

Overall, this work demonstrates that OAD is a feasible method to deposit tilted nanostructures in LSMO–Au VAN thin films. Previously, a special nanopillar design within the matrix was obtained either by selecting two materials with appropriate surface energy[28] or by single-layer OAD,[21] which could be limited in tailoring the pillar morphologies. Here, this study adopts a novel approach of rotational OAD, introducing a new method for tailoring Au nanostructures within the matrix. As evidenced in STEM images, different OAD angles result in very different Au nanostructures, while the LSMO matrix remains a continuous film. This is quite different from the LSMO nanocolumn formation *via* OAD growth of LSMO films.[29] The overall VAN thin films remain a continuous film with tilted Au nanopillars embedded in the LSMO matrix. In addition, by tuning the Au nanostructures to zigzag-shaped pillars or straight nanopillars by varying the inclination angle during deposition, all films exhibit a type-I optical hyperbolic behavior. These intriguing results offer a new material design option for photonic applications. Further work could include exploring versatile nanostructure designs *via* tuning the substrate rotation speed and the inclination angle during OAD. Other VAN systems with a large selection of oxide–metal combinations can be explored using the rotational OAD method for future specialized nanostructure configurations targeting specific applications.

Conclusion

This study demonstrates that OAD along with substrate rotation can be used to synthesize various Au nanostructures in self-assembled LSMO–Au VAN thin films. By varying the inclination angle of the substrate from 15° to 60°, the Au nanostructures vary from zigzagged pillars to vertical pillars, while the LSMO matrix remains a continuous film. By ellipsometry and angular-dependent reflectivity measurements, unique tunable hyperbolic properties have been demonstrated. The in-plane anisotropy has been demonstrated by measuring the samples upon in-plane rotation. This demonstration shows great potential for using rotational OAD to create different configurations of secondary phase embedded in a matrix for self-assembled hybrid metamaterials for future photonic device applications and many others.

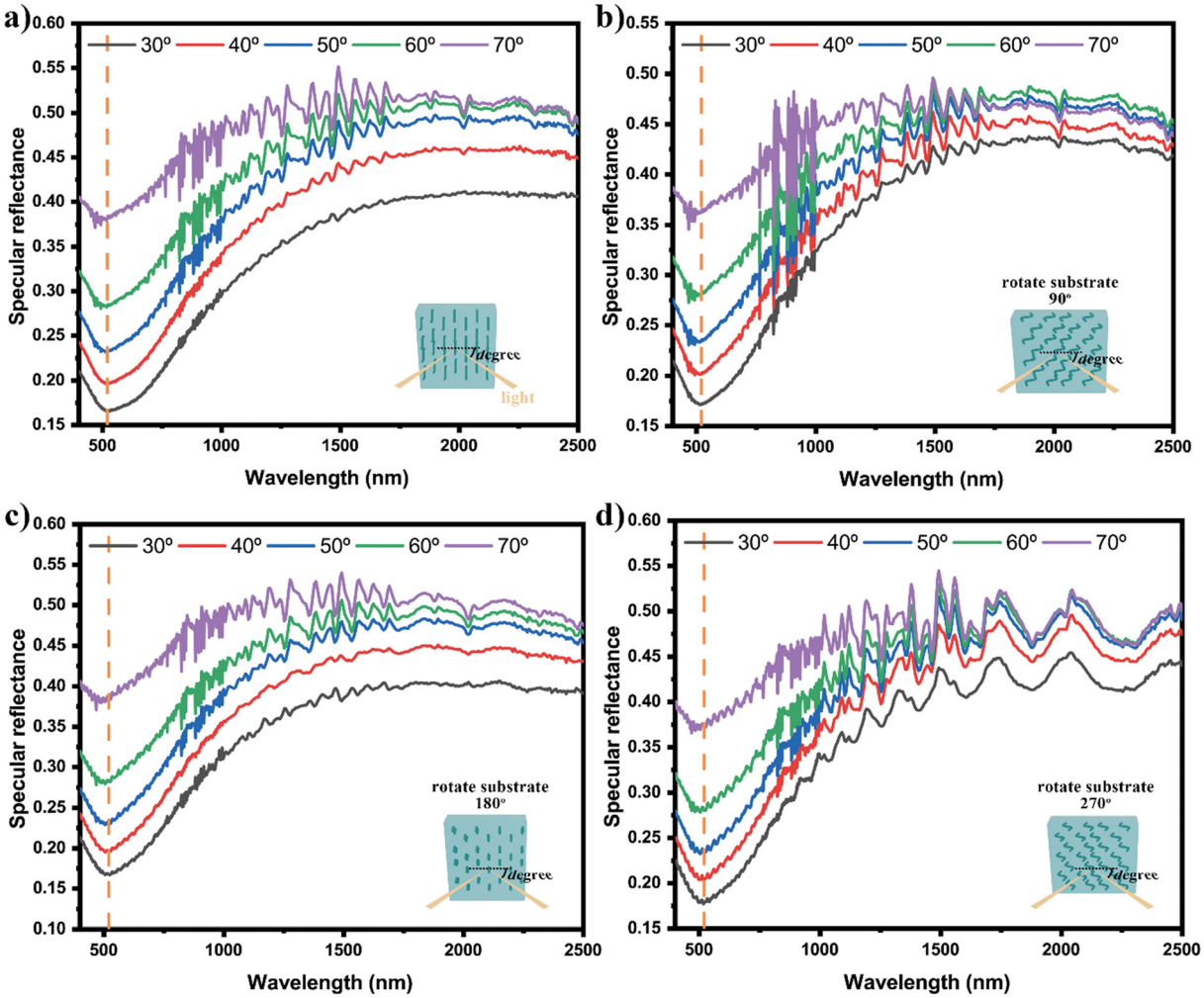

Fig. 5 In-plane angle-dependent reflectivity measurements, where light is incident at positive and negative angles. All rotation occurs in clockwise direction. a) 0° b) 90° c) 180° d) 360°.

Experimental methods

Synthesis of multifunctional thin film

The $La_{0.7}Sr_{0.3}MnO_3$ (LSMO) target was prepared by mixing MnO_2, La_2O_3, and $SrCO_3$ in stoichiometric proportions. The powder mixture is then pressed overnight into a pellet and sintered in a conventional tube furnace at 1300 °C for 10 hours. A 2 mm-wide Au strip is attached to the LSMO target. The substrate is attached at a desired angle (60°, 45°, 30°, and 15°) of the metal piece for achieving an oblique-angle deposition configuration. The film was grown on a $SrTiO_3$(001) substrate with deposition parameters of 450 mJ, a laser frequency of 5 Hz, a temperature of 700 °C, and an oxygen partial pressure of 100 mTorr.

Material characterization

X-ray diffraction (XRD, PANalytical Empyrean) was used to measure the crystallinity of all thin films. All thin films were prepared by mechanical grinding and polishing. After the desired thickness is obtained, argon-ion milling using a Gatan Precision Ion Milling System was used for final polishing. All high-angle annular dark-field scanning transmission electron microscopy (HAADF-STEM) images were obtained using a Thermo Fisher Scientific TALOS 200X TEM operated at 200 kV.

Author contributions

B. K. T. and H. W.: conceptualization, methodology, investigation, formal analysis, validation, visualization, writing – original draft. B. K. T., J. H., A. C. and H. W.: nanostructure characterization, formal analysis, writing – review & editing. A. C. and J. H.: optical property characterization. H. W.: conceptualization, methodology, writing – review & editing, project administration, funding acquisition, supervision, resources.

Conflicts of interest

There are no conflicts to declare.

Data availability

The additional data that support the findings of this study are available from the supplementary information (SI).

Supplementary information: including detailed XRD results and EDX mapping results for the samples deposited under different angles. See DOI: https://doi.org/10.1039/d6ce00284f.

Acknowledgements

This work is supported by the U.S. National Science Foundation (DMREF-2323752). J. G. and H. W. acknowledge support from the U.S. DOE Basic Energy Sciences (DE-SC0020077) for TEM sample preparation and imaging.

References

1 I. Liberal and N. Engheta, *Nat. Photonics*, 2017, **11**, 149–158, DOI: 10.1038/nphoton.2017.13.
2 N. Kinsey, C. DeVault, A. Boltasseva and V. M. Shalaev, *Nat. Rev. Mater.*, 2019, **4**, 742–760, DOI: 10.1038/s41578-019-0133-0.
3 N. Garcia, E. V. Ponizowskaya, H. Zhu, J. Q. Xiao and A. Pons, *Appl. Phys. Lett.*, 2003, **82**, 3147–3149, DOI: 10.1063/1.1569656.
4 A. Fang, T. Koschny and C. M. Soukoulis, *Phys. Rev. B: Condens. Matter Mater. Phys.*, 2009, **79**, 245127, DOI: 10.1103/PhysRevB.79.245127.
5 V. M. Shalaev, *Nat. Photonics*, 2007, **1**, 41–48, DOI: 10.1038/nphoton.2006.49.
6 C. M. Soukoulis and M. Wegener, *Nat. Photonics*, 2011, **5**, 523–530, DOI: 10.1038/nphoton.2011.154.
7 J. Yao, Z. Liu, Y. Liu, Y. Wang, C. Sun, G. Bartal, A. M. Stacy and X. Zhang, *Science*, 2008, **321**, 930, DOI: 10.1126/science.1157566.
8 J. Kanungo and J. Schilling, *Appl. Phys. Lett.*, 2010, **97**, 021903, DOI: 10.1063/1.3462311.
9 J. Song, D. Zhang, P. Lu, H. Wang, X. Xu, M. L. Meyerson, S. G. Rosenberg, J. Deitz, J. Liu and X. Wang, *et al.*, *Mater. Today Nano*, 2023, **22**, 100316, DOI: 10.1016/j.mtnano.2023.100316.
10 A. Choudhury, B. K. Tsai, P. Lu, D. Hermawan, L. Quigley, J. Huang, Z. Hu, J. Gan, N. G. Godinez and J. P. Barnard, *et al.*, *Small Sci.*, 2026, **6**, e202500622, DOI: 10.1002/smsc.202500622.
11 J. Huang, B. K. Tsai, A. Choudhury, J. Shen, C. A. Mihalko, S. Zhou, C. Liu and H. Wang, *Adv. Mater. Interfaces*, 2025, **12**, e00613, DOI: 10.1002/admi.202500613.
12 D. Zhang, S. Misra, L. Li, X. Wang, J. Jian, P. Lu, X. Gao, X. Sun, Z. Qi and M. Kalaswad, *et al.*, *Adv. Opt. Mater.*, 2020, **8**, 1901359, DOI: 10.1002/adom.201901359.
13 J. Huang, H. Wang, X. Wang, X. Gao, J. Liu and H. Wang, *ACS Appl. Mater. Interfaces*, 2020, **12**, 39920–39925, DOI: 10.1021/acsami.0c12935.
14 H. Zheng, J. Wang, S. E. Lofland, Z. Ma, L. Mohaddes-Ardabili, T. Zhao, L. Salamanca-Riba, S. R. Shinde, S. B. Ogale and F. Bai, *et al.*, *Science*, 2004, **303**, 661–663, DOI: 10.1126/science.1094207.
15 M. Kalaswad, B. Zhang, X. Wang, H. Wang, X. Gao and H. Wang, *Nanoscale Adv.*, 2020, **2**, 4172–4178, DOI: 10.1039/D0NA00405G.
16 Y. Zhang, J. Shen, B. K. Tsai, X. Sheng, Z. Hu, X. Zhang and H. Wang, *Small Methods*, 2024, **8**, 2400087, DOI: 10.1002/smtd.202400087.
17 J. Song, D. Zhang, M. Moceri, H. Dou, X. Zhang and H. Wang, *Adv. Mater. Interfaces*, 2024, **11**, 2400132, DOI: 10.1002/admi.202400132.
18 Y. He and Y. Zhao, *Nanoscale*, 2011, **3**, 2361–2375, DOI: 10.1039/C1NR10103J.
19 S. Bacheller, N. A. Welchert and M. Gupta, *Langmuir*, 2023, **39**, 1507–1514, DOI: 10.1021/acs.langmuir.2c02876.
20 A. Barranco, A. Borras, A. R. Gonzalez-Elipe and A. Palmero, *Prog. Mater. Sci.*, 2016, **76**, 59–153, DOI: 10.1016/j.pmatsci.2015.06.003.
21 Z. Qi, J. Tang, S. Misra, C. Fan, P. Lu, J. Jian, Z. He, V. G. Pol, X. Zhang and H. Wang, *Nano Energy*, 2020, **69**, 104381, DOI: 10.1016/j.nanoen.2019.104381.
22 J. Huang, H. Wang, Z. Qi, P. Lu, D. Zhang, B. Zhang, Z. He and H. Wang, *Nano Lett.*, 2021, **21**, 1032–1039, DOI: 10.1021/acs.nanolett.0c04213.
23 J. Lu, R. L. Paldi, Y. Pachaury, D. Zhang, H. Wang, M. Kalaswad, X. Sun, J. Liu, X. L. Phuah and X. Zhang, *et al.*, *Mater. Today Nano*, 2021, **15**, 100121, DOI: 10.1016/j.mtnano.2021.100121.
24 Y. Jiang, J. Guo, Y. Mi, W. Liang, S.-N. Luo, Y. Ji and J. Huang, *ACS Appl. Nano Mater.*, 2023, **6**, 342–350, DOI: 10.1021/acsanm.2c04454.
25 J. Huang, J. L. MacManus-Driscoll and H. Wang, *J. Mater. Res.*, 2017, **32**, 4054–4066, DOI: 10.1557/jmr.2017.281.
26 J. Patidar, A. Sharma, S. Zhuk, G. Lorenzin, C. Cancellieri, M. F. Sarott, M. Trassin, K. Thorwarth, J. Michler and S. Siol, *Surf. Coat. Technol.*, 2023, **468**, 129719, DOI: 10.1016/j.surfcoat.2023.129719.
27 S. Liedtke, C. Grüner, J. W. Gerlach, A. Lotnyk and B. Rauschenbach, *J. Vac. Sci. Technol., B*, 2018, **36**, 031804, DOI: 10.1116/1.5025013.
28 X. Wang, J. Jian, Z. Zhou, C. Fan, Y. Dai, L. Li, J. Huang, J. Sun, A. Donohue and P. Bermel, *et al.*, *Adv. Opt. Mater.*, 2019, **7**, 1801180, DOI: 10.1002/adom.201801180.
29 A. Chen, Z. Bi, C.-F. Tsai, L. Chen, Q. Su, X. Zhang and H. Wang, *Cryst. Growth Des.*, 2011, **11**, 5405–5409, DOI: 10.1021/cg200999s.